DOI: 10.1021/ma9026349

Macromolecules
ARTICLE

Facile Alignment of Amorphous Poly(ethylene oxide) Microdomains in a Liquid Crystalline Block Copolymer Using Magnetic Fields: Toward Ordered Electrolyte Membranes

Manesh Gopinadhan, Paweł W. Majewski, and Chinedum O. Osuji*

Department of Chemical Engineering, Yale University, New Haven, Connecticut 06520

Received November 29, 2009; Revised Manuscript Received January 20, 2010

ABSTRACT: Large area microdomain alignment in poly(ethylene oxide-*b*-6-(4′-cyanobiphenyl-4-yloxy) hexyl methacrylate) block copolymers was successfully accomplished by the application of a 6 T magnetic field while cooling from elevated temperatures in the melt state. Small-angle X-ray scattering demonstrated that lamellar and cylindrical PEO microdomains aligned with their interfaces along the applied field, whereas the smectic layers of the liquid crystalline mesophase are perpendicular to the field. This is in agreement with the positive diamagnetic anisotropy of the cyano-biphenyl mesogen and a homogeneous anchoring condition at the intermaterial dividing surface (IMDS) between the two blocks. The alignment of the system is driven by the diamagnetic anisotropy of the smectic mesophase and not by the crystallization of PEO at lower temperatures. The addition of poly(acrylic acid) and $LiClO_4$ salt result in the suppression of PEO crystallinity and stronger segregation between the polymer blocks leading to improved order in the material. The resulting films are well aligned over millimeter length scales of area and thickness. We use a novel continuous rotational annealing approach to break the degeneracy of the lamellar alignment, permitting facile directed assembly of the system during a single cooling step. Our experiments demonstrate the creation of well-aligned arrays of amorphous PEO domains over large length scales and offer a route to functional materials, in particular, for selective transport applications such as solid ionic electrolytes.

Introduction

Poly(ethylene oxide) (PEO) is a water-soluble semicrystalline polymer with many useful properties. It is heavily utilized as the hydrophilic segments in nonionic polymeric and oligomeric surfactants employed in nanomaterials synthesis[1,2] and complex fluid engineering.[3,4] In biological applications, PEO or poly(ethylene glycol) (PEG) is known for its inhibition of nonspecific protein adsorption and is used for passivation of surfaces that come into contact with biofluids.[5,6] Additionally, PEO has long been considered an attractive material in the design of polymer electrolytes for batteries. Most commonly, PEO is blended with lithium salts, forming an association complex between the ether oxygen and the lithium ion. The resulting material then functions as a lithium-conducting solid electrolyte for use in lithium ion batteries.[7−9]

The semicrystalline nature of PEO poses a problem for rapid ionic transport when the polymer is used as an electrolyte. Lithium ion conductivities decrease with the crystalline content of the system because of reduced segmental and chain mobility. Although crystallinity is generally suppressed by the addition of the lithium salt itself,[10,T1] increased lithium doping does not necessarily result in improved performance because the salt also increases the glass-transition temperature of the polymer and can form crystalline complexes at high stoichiometric ratios.[10,12,13] The result is that reasonable conductivities can only be achieved at temperatures above either the PEO crystalline melting temperature or the T_g of the system, or both, as relevant, where the PEO exists entirely in an amorphous highly mobile state. The drawback, however, is the inherently poor dimensional stability of such a fluid electrolyte and its susceptibility to damage by the growth of lithium dendrites during battery function.[14] As a result, from this perspective, the realization of all solid-state rechargeable lithium ion batteries remains a considerable challenge.

One way of overcoming this challenge is to employ nanostructured fluids that have good mechanical and dimensional stability globally, although composed of high mobility liquids locally. Block copolymers offer outstanding promise in this area. Microphase separation produces a system that displays the properties of the individual blocks on the nanoscale, but which responds as a material composite on a macroscopic level. For example, in poly(styrene-*b*-isoprene-*b*-styrene) triblock copolymers, locally, the poly(isoprene) microdomains are fluids with $T_g \approx -70$ °C, whereas the poly(styrene) domains are glassy with $T_g \approx 105$ °C. Macroscopically, however, the system is an elastomeric rubbery composite material produced by the combination of the glassy poly(styrene) and poly(isoprene) segments. The same concept has been applied in advancing PEO and other block copolymers for use as solid lithium electrolytes where dimensional stability is afforded by the block copolymer superstructure, whereas ionic conductivity is maintained in a locally fluid phase produced by salt doping.[15−20] The morphology of the system, however, becomes a key variable because good ionic conductivity depends on the provision of contiguous, nonconvoluted pathways from one side of the material to the other, entirely within the PEO domains. The high defect density and lack of long-range order that result on typical uncontrolled self-assembly of these materials thus pose significant problems for the utility of these systems as electrolytic membranes.

There is a strong need for the development of methods that enable facile control of ordering in these materials. Several approaches have been demonstrated for aligning block copolymer microstructures and controlling order in the materials. Shear flow, electric fields, directional solvent evaporation, thermal gradients, spatial confinement and chemical patterning, for

*Corresponding author. E-mail: chinedum.osuji@yale.edu.

 Published on Web 03/08/2010

example, as reviewed extensively,[21,22] have all shown to be effective in aligning block copolymers. The method chosen for a given application depends on the particular requirements as far as throughput, form factor, material compatibility, and so on. For the alignment of substrate-supported thin films (1−100 μm) on large length scales (> 1 mm), magnetic fields are particularly appealing because of their space pervasive nature, the absence of contact and field breakdown issues as encountered with electric fields, and the ease of effecting temperature control over the sample during the alignment. They rely on the presence of sufficient magnetic anisotropy in the system, such as is provided by the presence of a liquid crystalline mesophase in the materials. However, it has only been in recent years that a few reports of magnetic-field-driven alignment of block copolymer melts have begun to emerge.[23−29] Here we show that magnetic fields can be successfully used to generate well-aligned films of self-assembled PEO-based diblock copolymers. A liquid crystalline polymer forms the conjugate block, thus permitting field alignment. Crystallization of the PEO domains is successfully suppressed via formation of interpolymer complexes with poly(acrylic acid) (PAA) as well as by doping with lithium perchlorate ($LiClO_4$). Following a discussion of the phase behavior of the system, we show results for lamellar as well as cylindrical morphologies. We demonstrate that arbitrary alignment of the lamellar system may be accomplished by rotational annealing to break the typical degeneracy that results from field alignment of the lamellar morphology in these materials.

Experimental Section

Materials. Poly(ethylene oxide-*b*-6-(4′-cyanobiphenyl-4-yloxy)hexyl methacrylate) (EO-MA/LC) with molecular weight of 8.5 kg/mol (3.5k-*b*-5k) and polydispersity of 1.10 was obtained from Polymer Source, and 4′-(octyloxy)-4-biphenylcarbonitrile mesogen (307.43 g/mol) was obtained from Sigma-Aldrich. PAA (1.8 kg/mol) as well as $LiClO_4$ were purchased from Aldrich. All materials were used as received. The chemical structure of the block copolymer and carbonitrile mesogen are illustrated in Scheme 1. The homopolymer and free mesogen contents in blend samples were taken as percentages by weight with respect to the EO and MA/LC contents, respectively. Materials are referred to here as EO-MA/LC:(xAA)/(yfLC) where x and y are the weight percent composition of PAA and the free carbonitrile mesogen in the EO and MA/LC blocks, respectivley. Melt samples were prepared by slow evaporation of solvent from a 5 wt % solution of the copolymer in DMF at 65 °C. The films were vacuum-dried at 50 °C for 2 days and then used without further treatment.

Methods. Small-angle X-ray scattering (SAXS) experiments were performed using 1.54 Å radiation produced by a Cu anode microfocus source (Rigaku). Scattering was recorded using a gas-wire electronic area (2D) detector. The scattering vector, q, is defined as $q = (4\pi/\lambda) \sin \theta$, where 2θ is the scattering angle. The sample−detector distance was ca. 83 cm, permitting access to a range of scattering vectors from 0.016 to 0.3 Å^{-1}. SAXS diffractograms were calibrated using the scattering from silver behenate with d spacing of 58.38 Å. Automated temperature-controlled melt-state scattering was performed with a Linkam THMS 600 hot stage connected to a Linkam TMS 94 temperature controller. The samples were subjected to a heating rate of 5 °C/min with films held at the acquisition temperatures for 10 min prior to the measurements. DSC was conducted on a TA Instruments Q200 apparatus at a heating rate of 10 °C/min.

For magnetic alignment, small pieces of solvent-cast films about 1 to 2 mm thick and 3 mm in diameter were mounted on Kapton films that were placed in an aluminum sample holder. The sample holder was lowered into the constant field core region of a superconducting magnet (American Magnetics) at flux density of 6 T. Samples were heated to 110 °C, well above the liquid crystal clearing temperature and above the microphase order−disorder temperature in some cases, and then allowed to cool to room temperature at a rate of 0.12 °C/min. Temperature control was within 0.1 °C. Aligned samples were examined by polarized optical microscopy (POM) using a Zeiss Axio Observer microscope equipped with a Pike CCD camera. For POM, the samples were confined between two glass slides with a thin washer in between serving as a spacer to avoid any inadvertent shear-induced alignment. Measurements were made in transmission under crossed polarizers at 20× magnification.

Scheme 1. Molecular Structures of Poly(ethylene oxide-*b*-6-(4-cyanobiphenyl-4-yloxy)hexyl methacrylate) (EO-MA/LC) and 4′-(Octyloxy)-4-biphenylcarbonitrile

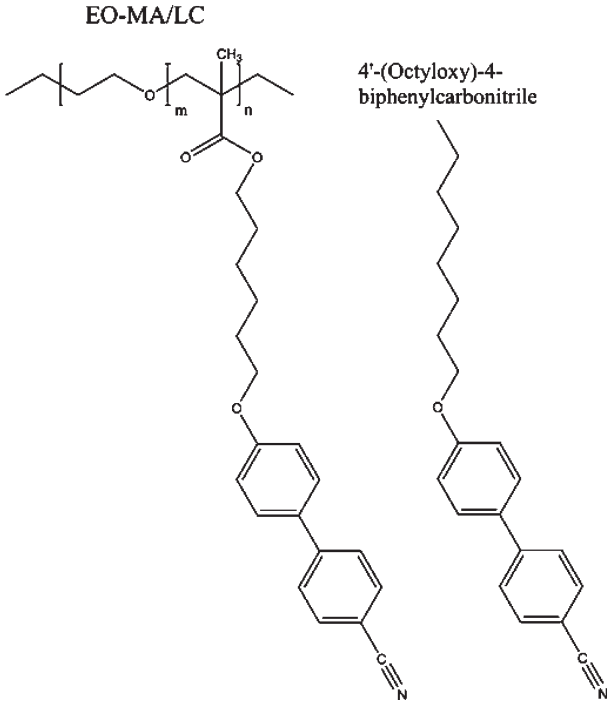

Results and Discussion

The neat diblock copolymer, EO-MA/LC, displayed a poorly ordered lamellar structure at room temperature, with a d spacing of 18.5 nm. The structure of the as-cast sample was significantly distorted by the crystallization of PEO, which was evidenced by large micrometer-scale spherulites that were visible under POM (Supporting Information, Figure 1). Upon heating, the PEO melted around 46 °C, resulting in slightly improved order of the lamellar microdomains and a corresponding sharper primary peak in SAXS (Figure 1). The material undergoes an order−disorder transition near 65 °C, beyond which there is only a weak correlation hole visible around $q = 0.039$ Å^{-1}. Upon subsequent cooling to 30 °C, the sample formed the lamellar morphology at $q = 0.046$ Å^{-1}, corresponding to a d spacing of 13.7 nm, but the PEO chains did not crystallize during the course of the SAXS measurement. This sharp reduction in the spacing is consistent with the initial formation of amorphous PEO domains. Slow isothermal crystallization at room temperature or accelerated crystallization with further undercooling would result in an increase in the d spacing due to additional chain stretching and enhanced segregation on crystallization of the PEO. Notably, the

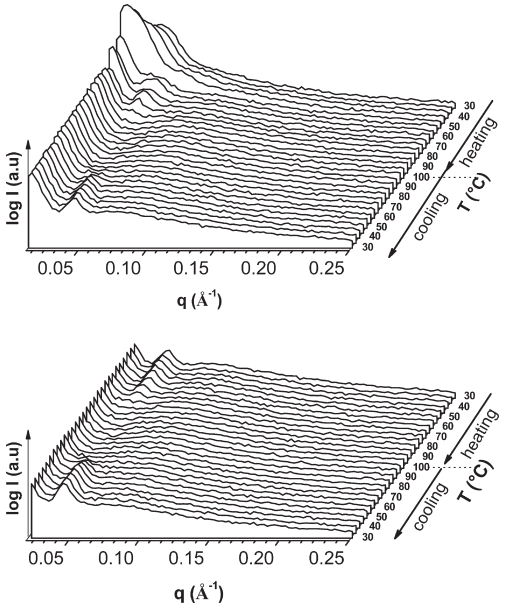

Figure 1. SAXS data of EO-MA/LC for the first and second heat−cool cycles at selected temperatures, as indicated. First heating shows a melting transition around 45 °C, and the subsequent cooling improves the order in the system. Both show an ODT around 70 °C.

scattering from the smectic layers at $q = 0.18$ Å^{-1}, $d = 3.5$ nm, is very weak, but its appearance and disappearance on heating and cooling are coincident with the order−disorder transition of the microphase-separated lamellar structure. Such thermotropic-induced microphase separation is not uncommon in low molecular weight systems such as the system under study.[29−31] A planar or homogeneous anchoring condition was inferred from ad-hoc and field-aligned samples, after suitable thermal relaxation, from the orthogonality of the lamellar scattering with respect to the smectic.[30]

The addition of PAA to the system results in the formation of an interpolymer complex between the PAA and the PEO block. Such complex formation is well known, in particular for the preparation of drug delivery microparticles using polyelectrolytes such as PVP, PMAA, and PSS and nonionic species such as PNVPyr and PEO.[32−34] Complexation between PEO and PAA has been demonstrated in PEO-PPO-PEO (Pluronic) triblock copolymers where the formation of the interpolymer complex dramatically improves the weak segregation between PEO and PPO domains, resulting in ordered structure formation in the melt state as well as suppression of PEO crystallization.[35] Similarly, here we find that the presence of PAA enhances the segregation between the low molar mass PEO and MA/LC domains, resulting in sharper Bragg peaks and more prominent scattering from the smectic layer structure for 10% PAA (Figure 2). There is a concomitant increase in the ODT of the system, from 63.7 to 70.5 °C, as shown in the data of Figure 3. There is a small increase in the *d* spacing of the lamellae, from 13.5 to 14.7 nm. Further addition of PAA, at 20%, results in the appearance of a strong second-order Bragg reflection, indicating further improvement in the order of the system (Figure 4). Instead of an ODT, as encountered for the neat diblock and 10% PAA samples, this material exhibits an order−order transition from lamellae to hexagonally packed cylinders around 70 °C, as evidenced by the change in the ratio of the peak locations from 1:2:3 to $\sqrt{1}$:$\sqrt{3}$:$\sqrt{4}$. There was no ODT detected over the experimental temperature range. The *d* spacing was unchanged, in agreement with previously reported results on PAA/Pluronics where sequential additions of PAA to the system were observed to have little effect on the domain spacing.[35] This is likely due to the highly collapsed nature of the interpolymer complex formed by the two polymers.

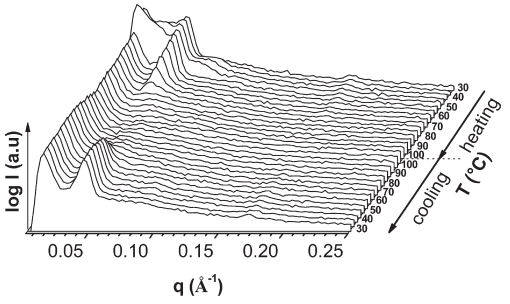

Figure 2. SAXS data as a function of temperature for EO-MA/LC:-(10AA) (second heat−cool cycle). The heating cycles show a melting transition around 45 °C and display an ODT around 70 °C.

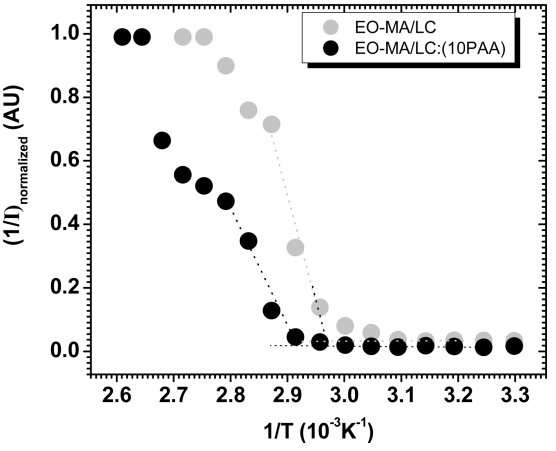

Figure 3. ODT for EO-MA/LC and EO-MA/LC:(10AA) is seen as change in peak intensity as a function of $1/T$ as represented.

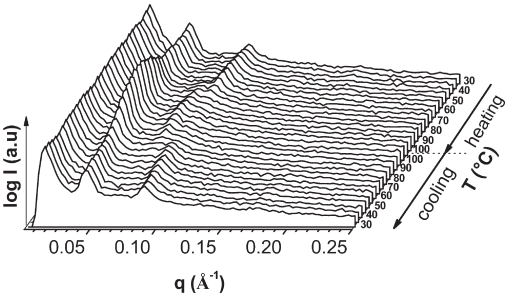

Figure 4. SAXS data as a function of temperature for EO-MA/LC:-(20AA) (second heat−cool cycle). The system displays an order−order transition (OOT) from a lamellar morphology to hexagonally packed cylinders around 70 °C.

Inclusion of 1% $LiClO_4$ by weight, corresponding to a stoichiometric ratio of [EO]/[Li] of 246:1, produced a further increase in the segregation between the EO and MA/LC domains, as inferred from the improved resolution of the structure in the SAXS. At this composition, the system again did not display an ODT over the experimental range, up to 110 °C (Figure 5). The clearing temperature of the LC, as determined by DSC, was relatively unchanged at 71.9 °C, compared with 71.3 °C for the neat diblock. The *d* spacing was again unchanged at 14.7 nm. Because of the unavailability, a neat diblock with the appropriate composition, blending with the free mesogenic species (fLC) (Scheme 1), was used to increase the volume fraction of the LC block to realize hexagonally packed cylindrical microstructures. Such blending of free mesogens has also been used in past work to

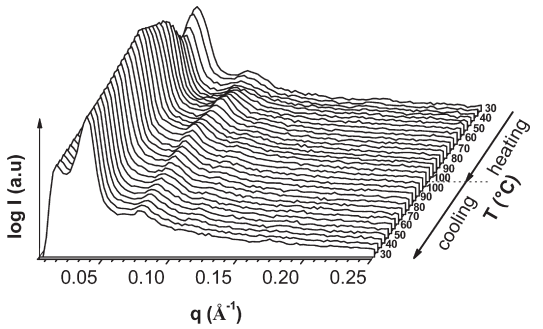

Figure 5. SAXS data as a function of temperature for EO-MA/LC:-(20AA + 1$LiClO_4$) (second heat−cool cycle). This system displays neither an ODT nor an OOT over the temperature range studied.

modify the morphology of poly(styrene-*b*-isoprene/LC) block copolymers.[36] The system was produced by adding 75% of 4′-(octyloxy)-4-biphenylcarbonitrile by weight relative to the MA/LC block to EO-MA/LC:(10AA). The resulting material, EO-MA/LC:(10AA)/(75fLC), was composed of hexagonally packed cylindrical microdomains of PEO with a d spacing of 14.5 nm. For hexagonally packed cylinders, the d spacing is related to the intercylinder distance, d_0 as $d_0 = (4/3)^{1/2}d$ and the volume fraction $\phi = (2\pi/\sqrt{3})(r/d_0)^2$. The volume fraction of the EO together with AA in the system is estimated from the weight fraction, $f_{EO:AA} = 0.29$, from which a cylinder radius of 4.7 nm and a cylinder-to-cylinder distance of 16.7 nm are inferred. The homogeneous anchoring condition of the mesophase was unchanged, and a smectic layer spacing of 3.5 nm was recorded, which is identical to that of the lamellar systems. From the absence of new scattering peaks and the conservation of the native smectic layer spacing, it can be concluded that the added mesogen simply coassembled with the existing mesophase formed by the covalently bonded moieties, resulting in a homogeneous swelling of the LC domains and the successful production of the cylindrical morphology.

DSC studies conducted at varying PAA/$LiClO_4$ concentrations reflect the trend of decreasing PEO crystallinity that is apparent from the low q regime of the SAXS data for the samples discussed above. As shown in Figure 6, there is a continuous decrease in the melting enthalpy with added PAA, normalized to the PEO content in the system. The enthalpies are normalized with respect to the melting enthalpy for the neat diblock, 9.216 J/g (22.42 J/g per EO). Compared with the enthalpy for completely crystalline PEO of roughly 200 J/g,[37,38] we observe that the confinement of the PEO blocks at ambient temperatures provides a starting point in which the system already displays reduced crystallinity. Significant suppression is driven by the formation of the interpolymer complex with PAA, and the inclusion of a relatively small amount of Li further decreases the crystalline content in the PEO domains.

In all cases, the materials prepared here were successfully aligned in the melt state by slowly cooling the samples at 0.12 °C /min in the presence of the 6 T field. The data for the neat diblock are shown in Figure 7. From an initially unoriented state, the application of the field vertically with respect to the scattering plane produces lamellae that are aligned with the IMDS along the field direction and smectic layers that are perpendicular to the field. The lamellar scattering is concentrated along the equatorial direction, and that due to the smectic layers is along the meridional line. That is, the director of the LC phase is parallel to the field and parallel to the lamellar IMDS, consistent with the homogeneous anchoring condition of the system, as schematically depicted in Figure 8. Given the dual properties of semicrystallinity and liquid crystallinity imparted by the PEO and PMA/LC blocks, respectively, there are two possible sources of

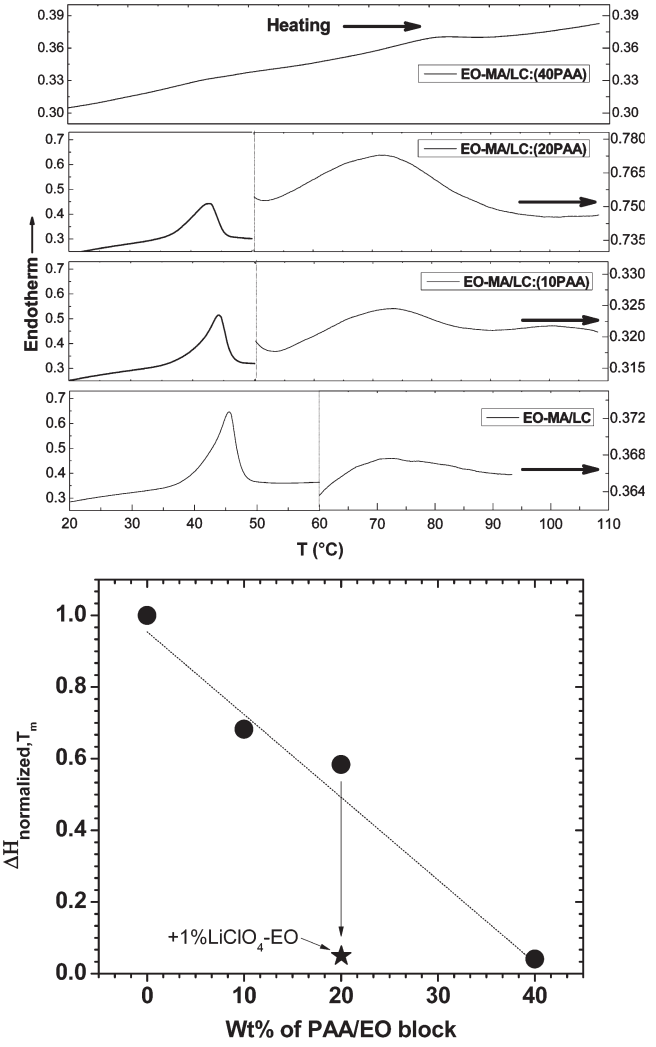

Figure 6. Top: DSC heat flow curves of EO-MA/LC samples at different compositions as indicated. The data scale is divided to display both the crystallization regime (left vertical axis) as well as the clearing transition of the smectic structure (right vertical axis). Bottom: Addition of PAA results in a reduction of the melting enthalpy. PAA composition is indicated as a weight percentage relative to the EO content. The enthalpies are normalized with respect to the melting enthalpy for the neat diblock by taking into account the PEO content in the system. Incorporation of $LiClO_4$ further reduces the crystallinity of the system.

the diamagnetic anisotropy that could drive alignment in the system. Magnetic alignment of a lamellar semicrystalline block copolymer, poly(ethylene oxide-*b*-butadiene), has been reported on the basis of field-directed PEO crystallization.[26] There, a 7 T field was applied during cooling through the crystallization temperature of the PEO, with the requirement that the system supported a high nucleation density to restrict the growth of spherulites and beyond their hedritic core and thus roughly maintain the diamagnetic anisotropy of the unit cell of the crystallized material.[39] Given the fairly low degrees of crystallinity in the present system, we expect that alignment here is driven by the diamagnetic anisotropy provided by the smectic mesophase. To test this, we cooled a sample under the field from 110 to 52 °C at 0.12 °C/min and then ramped down the field to zero while the temperature was held at 52 °C, which is well above the crystallization temperature for PEO. The sample was then permitted to cool to room temperature at the prior cooling rate but in the absence of the field such that any PEO crystallization would occur without a field bias. The data (Figure 7b) show well-aligned lamellae for sample EO-MA/LC, as was also produced

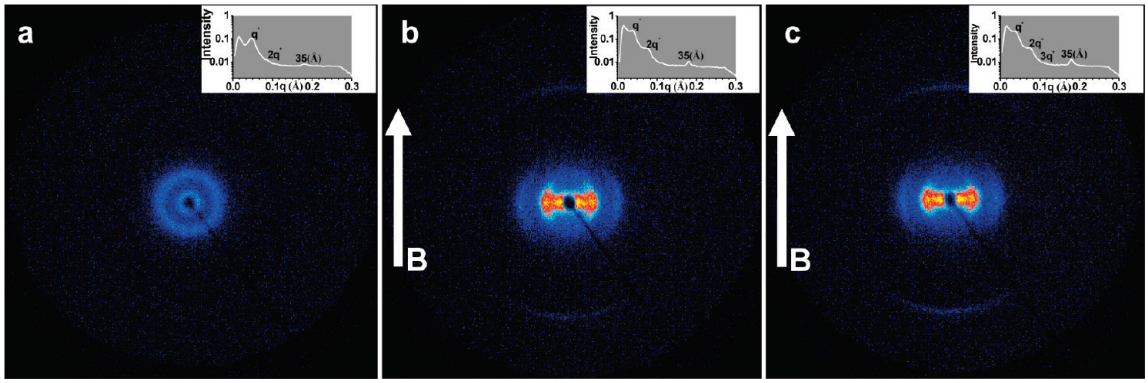

Figure 7. 2D scattering pattern of EO-MA/LC block copolymer: (a) no field; (b) the field (vertical) was switched off at 52 °C and the sample was allowed to cool in the absence of the field; and (c) field vertical to the plane when the sample was cooled down to room temperature from 110 °C. 2D images were rendered using WSxM software.[47]

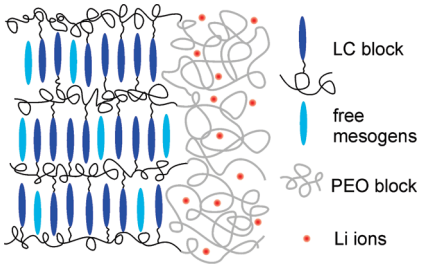

Figure 8. Schematic depiction of the arrangement of the block copolymer under a vertically applied magnetic field. Free mesogens are coassembled with the covalently bound mesogens in the LC block and are arranged with their long axis along the field and parallel to the interface with the PEO domain. Lithium ions are contained within the PEO domain, which also contains PAA chains (not shown) intimately associated with the PEO backbone.

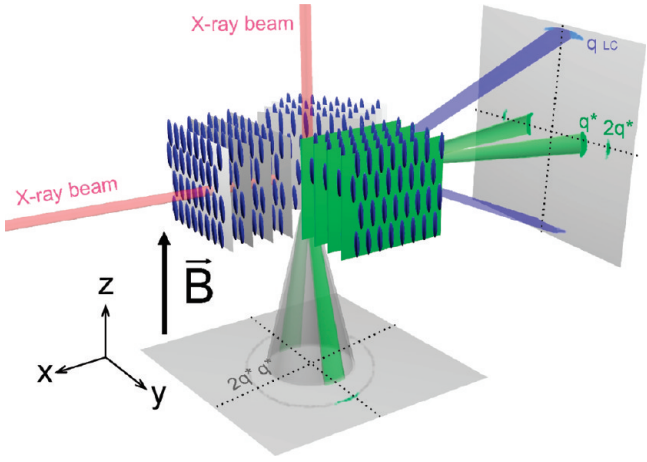

Figure 9. Magnetic alignment of lamellar microstructures depends on the anisotropy of magnetic susceptibility of the LC mesophase and the orientation of the mesogens (blue cigar-shaped objects) with respect to the IMDS. For the current system, the mesogens display homogeneous or planar anchoring and a positive diamagnetic anisotropy. Alignments that satisfy both the anchoring constraint and alignment, as dictated by the magnetic anisotropy, are degenerate, corresponding to the infinite possible orientations of lamellae with normals in the *xy* plane (three shown). From this degenerate set, only lamellae oriented with their layer normals perpendicular to the X-ray beam contribute to the scattering. With X-rays incident along the field, along the *z* axis, the entire lamellar set is under the Bragg condition, whereas the smectic layers are uniformly not in the Bragg condition. With X-rays incident along the *x* axis, only a small subset of lamellae (shaded green) contribute to the anisotropic scattering (also shaded green). Conversely, all smectic layers are now under the Bragg condition.

for samples cooled all the way to room temperature under the field. Although we cannot rule out a small additional influence of the field on the sample alignment during PEO crystallization, the low degree of crystallinity combined with the slow cooling procedure, which does not maximize nucleation site density, all strongly suggest that structure alignment here occurs because of the influence of the field on the LC mesophase.

These data do not give the complete picture, however. As shown in the schematic of Figure 9, parallel alignment of lamellar interfaces via a uniaxial field results in a degenerate situation. For a field along the *z* axis, the requirement that the lamellar interface be parallel to the field can be satisfied by any lamellae with their normals confined to the *xy* plane. The SAXS data discussed above are thus derived only from the small fraction of oriented lamellae that are in the Bragg condition for this geometry: only lamellae with layer normals along the *y* axis for X-rays incident along the *x* axis. Therefore, when the field is applied normal to the scattering plane, an isotropic ring should result as the large beam size (~0.5 mm) samples the orientations of many such degenerate lamellar assemblies. This corresponds to the situation depicted in Figure 9 with the beam incident along the *z* direction. This is precisely what is observed, as shown in Figure 10c for EO-MA/LC:(10AA). Consequently, the scattered intensity increases because all aligned lamellae are under the Bragg condition for this geometry. In this configuration, all aligned smectic layers are out of the Bragg condition and thus do not contribute to the scattering, hence the absence of the smectic signal. SAXS data were recorded for the other lamellar compositions studied at 10, 20, and 40% AA content and with lithium salt added to the 20% PAA blend, as shown in Figures 10−13a,respectively. POM was performed on aligned EO-MA/LC:(10AA) as a function of the angle between the field and the polarizer (Figure 14). A smooth variation was observed between the minima and maxima of the transmitted light intensities, which were separated by an angle of 45°. There is excellent separation between the normalized maxima and minima, indicating that the system is well aligned.

Degeneracy in the alignment of liquid crystalline mesophases has been noted before, for a side-chain liquid crystalline diblock copolymer based on a poly(styrene-*b*-isoprene) backbone.[24] In recent work, we have expanded on this description and demonstrated a novel technique, "rotational annealing", for the breaking of such degeneracy.[40] In this approach, a field rotation, or equivalently, a sample rotation, can be imposed to subject the sample to a time-averaged biaxial field that drives the selection of a unique or nondegenerate configuration of the system. Here rotation of the sample in the *yz* plane results in lamellae arranged with their normals along the *x* axis, the axis of rotation of the sample/field. This nondegenerate arrangement is made possible

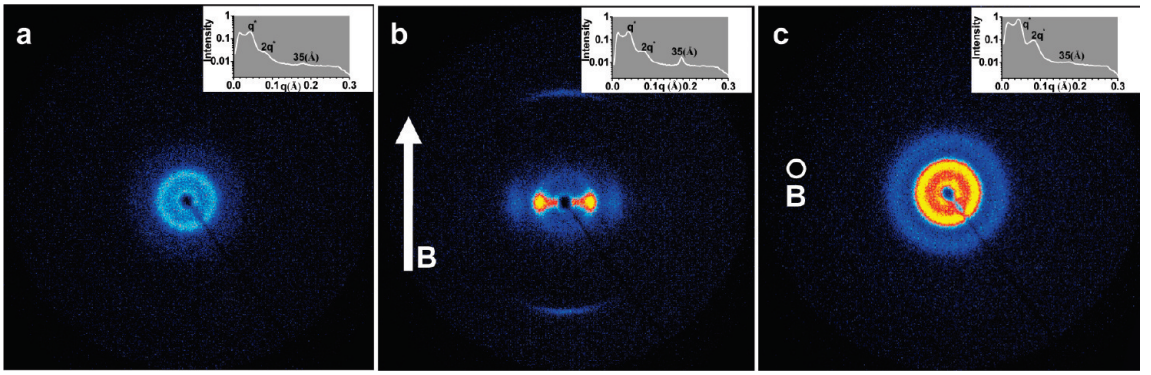

Figure 10. 2D scattering pattern of EO-MA/LC:(10AA) sample: (a) no field, (b) field in the vertical direction, and (c) field normal to the plane.

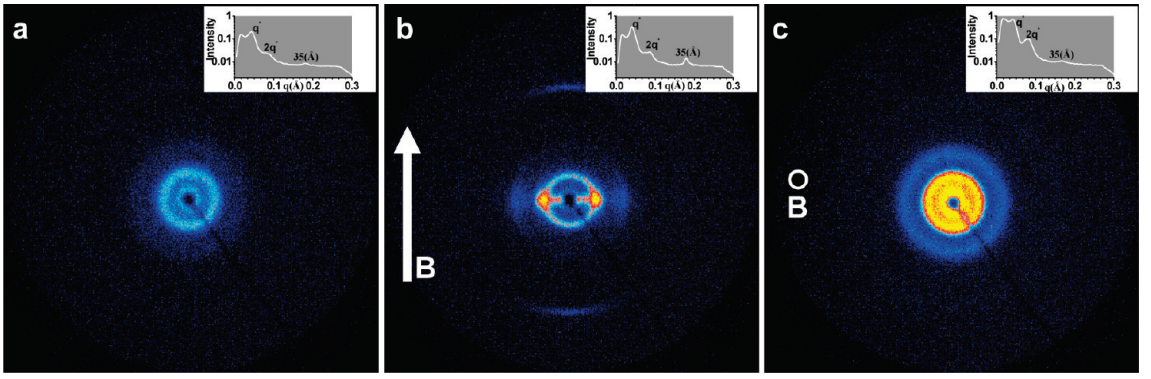

Figure 11. 2D scattering pattern of EO-MA/LC:(20AA) sample: (a) no field, (b) field in the vertical direction, and (c) field normal to the plane.

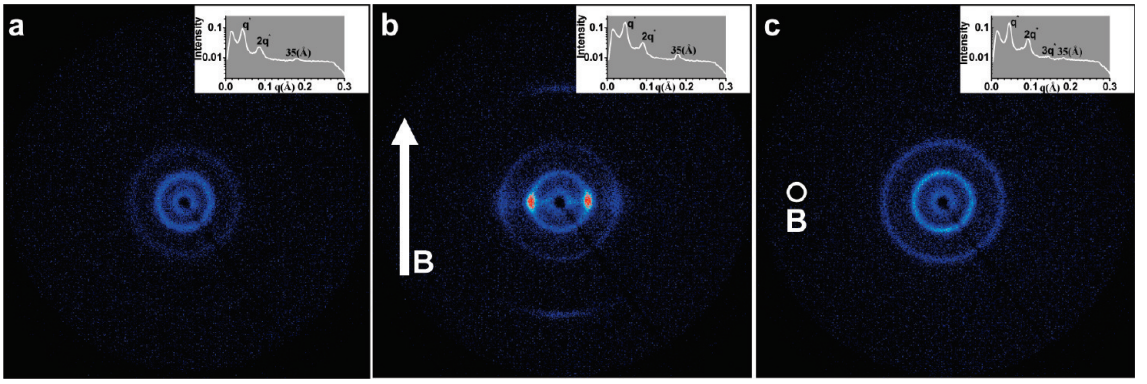

Figure 12. 2D scattering pattern of EO-MA/LC:(40AA) sample: (a) no field, (b) field in the vertical direction, and (c) field normal to the plane.

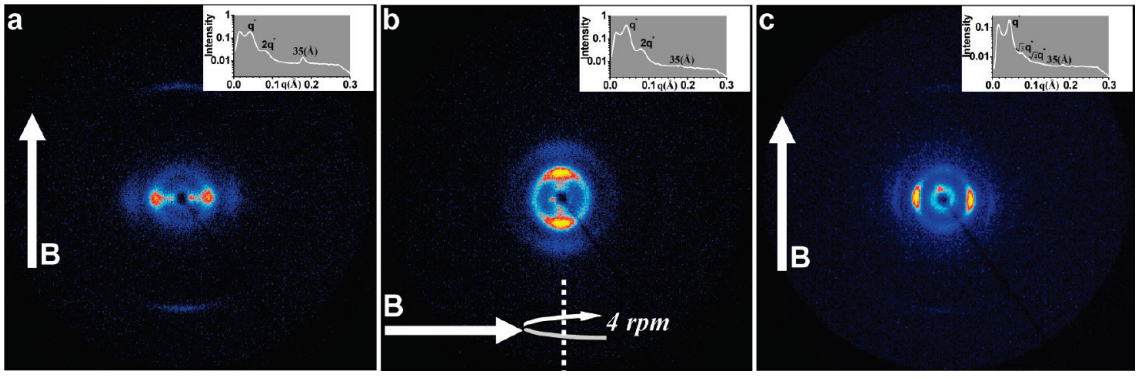

Figure 13. 2D scattering pattern of (a) EO-MA/LC:(20AA+1$LiClO_4$) sample when the field was vertical, (b) EO-MA/LC:(10AA) sample continuously rotated in the field at 4 rpm, and (c) the aligned cylindrical sample prepared by swelling the LC block of EO-MA/LC:(10AA) by incorporating of 4′-(octyloxy)-4-biphenylcarbonitrile.

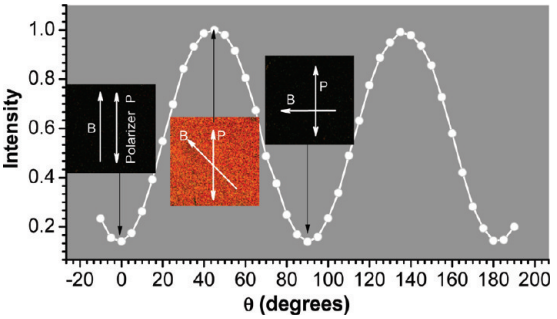

Figure 14. Transmitted intensity of the aligned EO-MA/LC:(10AA) sample under crossed polarized light plotted against the angle (θ) between the magnetic field direction and the polarizer shows periodic variation at every 90° indicating strong alignment of the mesogens along the field direction.

by the degeneracy implicit in the planar anchoring of the mesogens at the IMDS, which allows the system to select this as the lowest free-energy state. Only a small fraction of smectic layers will remain under the Bragg condition because of the freedom of the mesogens to rotate in the plane of the IMDS without breaking the planar anchoring constraint. We have applied this approach here, using a rotation of 4 rpm during the slow cooling ramp. As shown in Figure 13b, we observe the alignment of the lamellar microdomains as prescribed as well as the loss of the smectic scattering due to the degeneracy of the smectic ordering formerly described. The integral intensity resulting from alignment under rotation can be compared with that for uniaxial alignment by the field in the plane and perpendicular to the plane of scattering as limiting cases. The integral intensity is the integration within a small range over q and over all φ of the 2D scattering and is representative of the number density of lamellae in the Bragg condition, eq 1. Data are normalized with respect to the integral intensity produced for an in-plane alignment, set to 1.0. On the basis of the alignment of the EO-MA/LC:(10AA) sample, we calculate $I_{\text{perpendicular}} = 3.7$, whereas $I_{\text{rotated}} = 3.3$. These data indicate that there is a significant increase in the number of scattering lamellae due to the breaking of the degeneracy of the system, relative to the simple in-plane case. The procedure, however, still needs to be tuned to find the right combination of cooling rate and rotation speed to optimize the alignment produced.

$$I^{I} = \int_{q-\varepsilon_q}^{q+\varepsilon_q} \int_{0}^{2\pi} I(q,\varphi)\, \mathrm{d}q\, \mathrm{d}\varphi \tag{1}$$

Because of the curvature of the IMDS in the cylindrical case, the hexagonally packed cylindrical morphology does not suffer from the same degeneracy issue as does the lamellar morphology for planar anchoring and a positive diamagnetic anisotropy of the mesophase.[40] The alignment of the cylinder-forming sample EO-MA/LC:(10AA)/(75fLC) is shown by the SAXS data of Figure 13c.

It is worthwhile to compare the magnitude of the driving forces for magnetic alignment to those produced by the application of electric fields. The free-energy density difference between parallel and perpendicular arrangements of lamellae under an electric field is given by eq 2 and by eq 3 for a magnetic field.

$$|\Delta F_E| = \frac{1}{2} E^2 \Delta\varepsilon\varepsilon_0 \tag{2}$$

$$|\Delta F_B| = \frac{B^2 \Delta\chi}{2\mu_0} \tag{3}$$

For the electric field case, $\Delta\varepsilon$ is the dielectric anisotropy between parallel and perpendicular lamellar orientations, ε_0 is the dielectric permittivity of free space, and E is the electric field or potential gradient.[41,42] In the magnetic case, $\Delta\chi$ is the anisotropy of magnetic susceptibility, μ_0 is the magnetic permeability of free space, and B is the magnetic field strength of field intensity, measured in Tesla. Using the prototypical example of poly(styrene) and poly(methyl methacrylate), the free-energy density difference ranges from 0.54 to 3.9×10^{22} m^{-3} in units of kT at 298 K, depending on the particular values chosen for the dielectric constants of PS and PMMA and at a field of 10 V/μm.[43−46] To overcome thermal energy, coherent domains ranging in size from 30 to 58 nm must be present in the system. By comparison, at a field of 6 T, using a representative value of 5×10^{-7} for the volume diamagnetic anisotropy for thermotropic aromatic LCs and taking into account the volume fraction of the LC phase, the free-energy density difference amounts to 4.4×10^{20} m^{-3} kT. For this energy density, coherent domains of 132 nm are required to overcome thermal energy.

Conclusions

Our work has demonstrated that self-assembled lamellar and hexagonally packed cylindrical PEO microdomains in a liquid crystalline block copolymer can be successfully aligned using a magnetic field. Alignment for this system is driven by diamagnetic anisotropy that originates because of the smectic ordering of the mesogens in the liquid crystalline block and not because of the crystallization of the ethylene oxide units. Crystallization of the PEO block was substantially suppressed by the formation of an interpolymer complex with PAA as well as by the addition of lithium perchlorate, which also complexes with the PEO chains. The addition of these dopants resulted in enhanced segregation between the EO and MA/LC blocks, which gave rise to improved long-range order in the microphase-separated structures formed, and a concomitant increase in the order−disorder transition temperature for the system. Importantly, the presence of the dopants did not adversely affect the ability to align the system by the magnetic field. We have shown that rotational annealing can be applied effectively here to break the degeneracy of the alignment of the lamellar microdomains, enabling in principle arbitrary alignments of lamellae to be produced with respect to a substrate by simply controlling the substrate orientation with respect to the magnetic field. Future work will focus on alignment kinetics and the modification of phase behavior because of the application of the magnetic field. Here custom synthesized materials will be utilized to permit independent access to the lamellar- and cylinder-forming regimes of the phase diagram without the need for blending.

The ability to produce alignment of self-assembled structures over large length scales and in a facile manner is key to the application of block copolymers in a host of emerging areas. Magnetic field-driven alignment is well-suited to this challenge in areas where strong flow fields or intricate topological constraints cannot be imposed on the sample to control ordering. The control demonstrated over the alignment of PEO is particularly interesting given the potential applications of ordered PEO domains in thin films as ionic transport media for use in solid battery electrolytic membrane. The results of this work should spur new developments in this area.

Acknowledgment. This work was funded by the National Science Foundation under DMR-0847534. C.O. and M.G. acknowledge support from the Yale Institute for Nanoscience and Quantum Engineering (YINQE).

Supporting Information Available: Optical micrograph of the neat diblock copolymer at room temperature showing spherulites due to PEO crystallization. This material is available free of charge via the Internet at http://pubs.acs.org.

References and Notes

(1) Sakai, T.; Alexandridis, P. *Langmuir* **2004**, *20*, 8426–8430.
(2) Qi, L. M.; Ma, J. M.; Cheng, H. M.; Zhao, Z. G. *J. Phys. Chem. B* **1997**, *101*, 3460–3463.
(3) Alexandridis, P. *Curr. Opin. Colloid Interface Sci.* **1997**, *2*, 478–489.
(4) Almgren, M.; Brown, W.; Hvidt, S. *Colloid Polym. Sci.* **1995**, *273*, 2–15.
(5) Ratner, B. D.; Bryant, S. J. *Annu. Rev. Biomed. Eng.* **2004**, *6*, 41–75.
(6) Jon, S. Y.; Seong, J. H.; Khademhosseini, A.; Tran, T. N. T.; Laibinis, P. E.; Langer, R. *Langmuir* **2003**, *19*, 9989–9993.
(7) Croce, F.; Appetecchi, G. B.; Persi, L.; Scrosati, B. *Nature* **1998**, *394*, 456–458.
(8) Song, J. Y.; Wang, Y. Y.; Wan, C. C. *J. Power Sources* **1999**, *77*, 183–197.
(9) Wright, P. V. *MRS Bull.* **2002**, *27*, 597–602.
(10) Young, W. S.; Epps, T. H. *Macromolecules* **2009**, *42*, 2672–2678.
(11) Guilherme, L. A.; Borges, R. S.; Moraes, E. M. S.; Silva, G. G.; Pimenta, M. A.; Marletta, A.; Silva, R. A. *Electrochim. Acta* **2007**, *53*, 1503–1511.
(12) MacGlashan, G. S.; Andreev, Y. G.; Bruce, P. G. *Nature* **1999**, *398*, 792–794.
(13) Lightfoot, P.; Mehta, M. A.; Bruce, P. G. *Science* **1993**, *262*, 883–885.
(14) Brissot, C.; Rosso, M.; Chazalviel, J. N.; Lascaud, S. *J. Power Sources* **1999**, *81*, 925–929.
(15) Soo, P. P.; Huang, B. Y.; Jang, Y. I.; Chiang, Y. M.; Sadoway, D. R.; Mayes, A. M. *J. Electrochem. Soc.* **1999**, *146*, 32–37.
(16) Ruzette, A. V. G.; Soo, P. P.; Sadoway, D. R.; Mayes, A. M. *J. Electrochem. Soc.* **2001**, *148*, A537–A543.
(17) Ghosh, A.; Kofinas, P. *J. Electrochem. Soc.* **2008**, *155*, A428–A431.
(18) Singh, M.; Odusanya, O.; Wilmes, G. M.; Eitouni, H. B.; Gomez, E. D.; Patel, A. J.; Chen, V. L.; Park, M. J.; Fragouli, P.; Iatrou, H.; Hadjichristidis, N.; Cookson, D.; Balsara, N. P. *Macromolecules* **2007**, *40*, 4578–4585.
(19) Park, M. J.; Balsara, N. P. *Macromolecules* **2008**, *41*, 3678–3687.
(20) Wanakule, N. S.; Panday, A.; Mullin, S. A.; Gann, E.; Hexemer, A.; Balsara, N. P. *Macromolecules* **2009**, *42*, 5642–5651.
(21) Darling, S. B. *Prog. Polym. Sci.* **2007**, *32*, 1152–1204.
(22) Park, C.; Yoon, J.; Thomas, E. L. *Polymer* **2003**, *44*, 6725–6760.
(23) Galli, G.; Chiellini, E.; Francescangeli, O.; Ferri, D.; Wolff, D.; Springer, J.; Laus, M.; Angeloni, A. S. *Macromol. Symp.* **1997**, *121*, 235–244.
(24) Osuji, C.; Ferreira, P. J.; Mao, G. P.; Ober, C. K.; Vander Sande, J. B.; Thomas, E. L. *Macromolecules* **2004**, *37*, 9903–9908.
(25) Tao, Y. F.; Zohar, H.; Olsen, B. D.; Segalman, R. A. *Nano Lett.* **2007**, *7*, 2742–2746.
(26) Grigorova, T.; Pispas, S.; Hadjichristidis, N.; Thurn-Albrecht, T. *Macromolecules* **2005**, *38*, 7430–7433.
(27) Tomikawa, N.; Lu, Z. B.; Itoh, T.; Imrie, C. T.; Adachi, M.; Tokita, M.; Watanabe, J. *Jpn. J. Appl. Phys., Part 2* **2005**, *44*, L711–L714.
(28) Xu, B.; Pinol, R.; Nono-Djamen, M.; Pensec, S.; Keller, P.; Albouy, P. A.; Levy, D.; Li, M. H. *Faraday Discuss.* **2009**, *143*, 235–250.
(29) Hamley, I. W.; Castelletto, V.; Lu, Z. B.; Imrie, C. T.; Itoh, T.; Al-Hussein, M. *Macromolecules* **2004**, *37*, 4798–4807.
(30) Osuji, C. O.; Chen, J. T.; Mao, G.; Ober, C. K.; Thomas, E. L. *Polymer* **2000**, *41*, 8897–8907.
(31) Zheng, W. Y.; Hammond, P. T. *Macromolecules* **1998**, *31*, 711–721.
(32) Bokias, G.; Staikos, G.; Iliopoulos, I.; Audebert, R. *Macromolecules* **1994**, *27*, 427–431.
(33) Khutoryanskiy, V. V.; Dubolazov, A. V.; Nurkeeva, Z. S.; Mun, G. A. *Langmuir* **2004**, *20*, 3785–3790.
(34) Bell, C. L.; Peppas, N. A. *Biopolymers II*; Advances in Polymer Science *122*; Springer: New York, 1995; pp 125−175.
(35) Tirumala, V. R.; Romang, A.; Agarwal, S.; Lin, E. K.; Watkins, J. J. *Adv. Mater.* **2008**, *20*, 1603−1608.
(36) O'Rourke, M. J. In *Materials Science and Engineering*; Massachusetts Institute of Technology: Cambridge, U.K., 2003.
(37) Li, X.; Hsu, S. L. *J. Polym. Sci., Part B: Polym. Phys.* **1984**, *22*, 1331–1342.
(38) Richardson, P. H.; Richards, R. W.; Blundell, D. J.; Macdonald, W. A.; Mills, P. *Polymer* **1995**, *36*, 3059–3069.
(39) Ebert, F.; Thurn-Albrecht, T. *Macromolecules* **2003**, *36*, 8685–8694.
(40) Majewski, P. W.; Osuji, C. O. *Soft Matter* **2009**, *5*, 3417–3421.
(41) Pereira, G. G.; Williams, D. R. M. *Macromolecules* **1999**, *32*, 8115–8120.
(42) DeRouchey, J.; Thurn-Albrecht, T.; Russell, T. P.; Kolb, R. *Macromolecules* **2004**, *37*, 2538–2543.
(43) Amundson, K.; Helfand, E.; Quan, X. N.; Hudson, S. D.; Smith, S. D. *Macromolecules* **1994**, *27*, 6559–6570.
(44) Xu, T.; Zvelindovsky, A. V.; Sevink, G. J. A.; Lyakhova, K. S.; Jinnai, H.; Russell, T. P. *Macromolecules* **2005**, *38*, 10788–10798.
(45) Xu, T.; Zhu, Y. Q.; Gido, S. P.; Russell, T. P. *Macromolecules* **2004**, *37*, 2625–2629.
(46) Thurn-Albrecht, T.; DeRouchey, J.; Russell, T. P.; Kolb, R. *Macromolecules* **2002**, *35*, 8106–8110.
(47) Horcas, I.; Fernandez, R.; Gomez-Rodriguez, J. M.; Colchero, J.; Gomez-Herrero, J.; Baro, A. M. *Rev. Sci. Instrum.* **2007**, *78*, 013705.